journal of the mechanical behavior of biomedical materials 134 (2022) 105411

Contents lists available at ScienceDirect

Journal of the Mechanical Behavior of Biomedical Materials

journal homepage: www.elsevier.com/locate/jmbbm

Development of robust finite element models to investigate the stability of osteochondral grafts within porcine femoral condyles

Gavin A. Day *, Robert J. Cooper, Alison C. Jones, Marlène Mengoni, Ruth K. Wilcox

Institute of Medical and Biological Engineering, Mechanical Engineering, University of Leeds, UK

ARTICLE INFO

Keywords:
Cartilage
Bone
Finite element analysis
Knee
Modelling
Osteoarthritis
Surgical repair

ABSTRACT

Osteoarthritis (OA) is the most prevalent chronic rheumatic disease worldwide with knee OA having an estimated lifetime risk of approximately 14%. Autologous osteochondral grafting has demonstrated positive outcomes in some patients, however, understanding of the biomechanical function and how treatments can be optimised remains limited. Increased short-term stability of the grafts allows cartilage surfaces to remain congruent prior to graft integration. In this study methods for generating specimen specific finite element (FE) models of osteochondral grafts were developed, using parallel experimental data for calibration and validation. Experimental testing of the force required to displace osteochondral grafts by 2 mm was conducted on three porcine knees, each with four grafts. Specimen specific FE models of the hosts and grafts were created from registered μCT scans captured from each knee (pre- and post-test). Material properties were based on the μCT background with a conversion between μCT voxel brightness and Young's modulus. This conversion was based on the results of the separate testing of eight porcine condyles and optimization of specimen specific FE models. The comparison between the experimental and computational push-in forces gave a strong agreement with a concordance correlation coefficient (CCC) = 0.75, validating the modelling approach. The modelling process showed that homogenous material properties based on whole bone BV/TV calculations are insufficient for accurate modelling and that an intricate description of the density distribution is required. The robust methodology can provide a method of testing different treatment options and can be used to investigate graft stability in full tibiofemoral joints.

1. Introduction

Osteoarthritis (OA) is the most prevalent chronic rheumatic disease with knee OA having an estimated lifetime risk of 14 percent worldwide (Bortoluzzi et al., 2018). Conservative treatments for OA are suggested to be ineffective for both pain relief and prevention to disease progression, and fail to be cost effective (Crawford et al., 2013). Osteochondral defects to weight-bearing articular surfaces present an increasing challenge in healthcare, with patients experiencing pain, swelling, and instability that can lead to early degenerative changes. A number of surgical interventions exist that aim to restore the articulating surfaces of the joint. These include microfracture (Hunziker, 2002), autologous or allogeneic osteochondral grafts, and cell based approaches such as chondrocyte implantation. Larger regions of cartilage damage are often treated with partial or total joint replacement (Seo et al., 2011).

Osteochondral grafts that can be implanted into the site of the defect, flush with the cartilage surface, allow a restoration of the articulating surface (Kock et al., 2008; Pearce et al., 2001; Koh et al., 2004). The use of osteochondral grafts clinically involves the implantation of single or multiple grafts (mosaicplasty) to restore the articular cartilage such that the now congruent surface leads to a reduction in contact pressure (Seo et al., 2011). The advantage of osteochondral grafting is that it provides an immediate restoration of the cartilage surface and does not rely solely on inducing a cartilage repair response as with microfracture and cell based treatments (Hunziker, 2002). Clinical limitations of the grafting treatment surround tissue availability, donor site morbidity, and the lack of osseointegration between graft and the host material. While osteochondral grafts have been used to treat articular cartilage defects successfully, literature on their mechanical response and stability remains limited (Bowland et al., 2020). Additionally, the success of the treatment relies on the maintenance of a congruent surface during weight-bearing (Pearce et al., 2001). Therefore, it is important that the grafts do not subside prior to integration with the host. The correct positioning and angle of the grafts with respect to the surrounding

* Corresponding author.
E-mail address: g.day1@leeds.ac.uk (G.A. Day).

https://doi.org/10.1016/j.jmbbm.2022.105411
Received 5 November 2021; Received in revised form 21 July 2022; Accepted 5 August 2022
Available online 8 August 2022

cartilage surface has been shown to be challenging (Martinez-Carranza et al., 2013), with increased contact pressures found for grafts at incorrect angles (Koh et al., 2006). The general consensus is that the grafts should be placed flush or just below the articular surface (Martinez-Carranza et al., 2013; Manda et al., 2011; Kirker-Head et al., 2006; Custers et al., 2007; Becher et al., 2008), with deeper placement having been shown to be damaging (Martinez-Carranza et al., 2013; Manda et al., 2011; Custers et al., 2007).

Experimentally, the stability, tribological behaviour, and other performance metrics of osteochondral grafting have been identified through uniaxial push-in tests (Bowland et al., 2020), reciprocating pin-on-plate friction simulators (Bowland et al., 2018a, 2018b), and testing of tibiofemoral joints following treatment (Kock et al., 2008). However, stratification of grafts and hosts, and isolating the effect of wide ranging material properties within the population can be difficult. Computational approaches to understanding the environment of osteochondral grafts and their hosts (Manda et al., 2011; D'Lima D et al., 2009; Wu et al., 2002; Heuijerjans et al., 2018; Ovesy et al., 2020) have so far not investigated the material properties of the grafts or attempted to replicate the push-in force and short term stability.

The aim of this study was to develop a robust method for generating specimen-specific models of an osteochondral graft within a femoral condyle for examining the short term stability of the graft prior to osseointegration. The focus of this work was to confirm the requirement for detailed bone property information and demonstrate how closely models with mapped bone materials can match experimental push-in testing.

2. Methodology

Three main arms of testing were used to create and validate the FE models that mimicked the push-in tests, these are detailed in Fig. 1. The first two arms consisted of the derivation of material properties and mapping, and the derivation of the coefficient of friction values. The last arm consisted of experimental push-in tests to acquire scan and force data, from which the FE models were created and validated. These methods, both experimental and computational, are described in this section. Material and coefficient of friction values for the different FE models used in this study are found in Table 1.

2.1. Derivation of material property mapping

An accurate conversion between the brightness value of each voxel from the μCT scan and the Young's modulus of each element in the FE model was required to describe the material properties correctly. Many aspects of the model rely on having appropriate material properties for the bone, including the compression of the bone during push-in, the resultant press-fit from the graft oversizing and the friction between graft and host (which is a function of the graft oversize and material properties as well as the coefficient of friction). The sensitivity to these material properties is investigated in section 2.3.3. Material property mapping is achieved through a conversion from the brightness of a μCT voxel to a Young's modulus using an optimised linear constant. The voxel brightness is directly correlated to the bone density of the region via the segmentation, binarisation and downsampling process described below.

2.1.1. Experimental model and imaging

Four porcine skeletally immature 4- to 6- month old femurs were sourced from a local abattoir and were kept hydrated throughout the preparation and testing using phosphate buffered saline (PBS; MP Biomedicals LLC, UK). Samples were stored in PBS soaked tissue in a 4 °C fridge and all testing was carried out within one day. The femurs were dissected from the knee and cut such that the shape resembled that in Fig. 2, the condyles were then halved and the cartilage surface was removed using a scalpel. Each condyle was potted separately in polymethyl methacrylate (PMMA) cement as shown in Fig. 2. The eight potted specimens were tested using a materials testing machine (Instron 3365 with a 5 kN load cell, Instron, UK), with a load applied between two flat platens. A preconditioning (Zhao et al., 2018), cyclic load to 100 N was applied 10 times, which ensured that an applied force gave a consistent displacement, indicating that the bone had bedded into the endcaps correctly and that any short-term viscoelastic effects in both the bone and any remaining soft tissue had been removed. A load of 1000 N

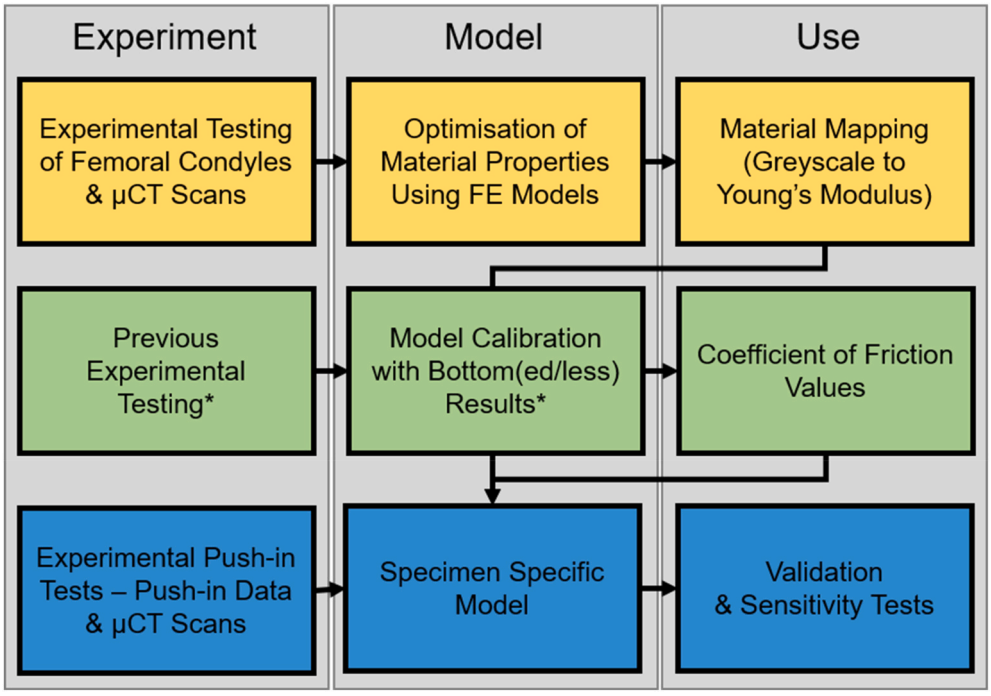

Fig. 1. *An overview of the three main arms of computational and experimental testing that were used to build the final FE model; yellow: derivation of material properties and mapping, green: derivation of the coefficient of friction values and blue: the push-in test. * Results from Bowland* et al. (Bowland et al., 2020).

Table 1
Coefficient of friction and material properties used for the different types of FE models used in the study.

	Material Property Mapping Models	Simplified Model	Graft Material Property Dependence		Graft Oversizing Material Properties	Final Model
			Specimen Specific Homogenous	Uniform Homogenous		
Coefficient of Friction Values						
Bone - Bone	N/A	Used to calibrate	0.21	0.21	0.21	0.21
Cartilage - Bone	N/A	Used to calibrate	0.14	0.14	0.14	0.14
Cartilage - Cartilage	N/A	Used to calibrate	0.1	0.1	0.1	0.1
Material Properties						
Bone Properties - Host (MPa)	Used to calibrate	80	92.8 × BV/TV	92.8 × BV/TV	92.8 × BV/TV	92.8 × BV/TV
Cartilage Properties - Host (MPa)	N/A	Neo-Hookean K = 16.67, G = 1.37.	Neo-Hookean K = 16.67, G = 1.37.	Neo-Hookean K = 16.67, G = 1.37.	Neo-Hookean K = 16.67, G = 1.37.	Neo-Hookean K = 16.67, G = 1.37.
Bone Properties - Graft (MPa)	N/A	80	67	92.8 × mean BV/TV for each graft	92.8 × BV/TV	92.8 × BV/TV
Cartilage Properties - Graft (MPa)	N/A	Neo-Hookean K = 16.67, G = 1.37.	Neo-Hookean K = 16.67, G = 1.37.	Neo-Hookean K = 16.67, G = 1.37.	Neo-Hookean K = 16.67, G = 1.37.	Neo-Hookean K = 16.67, G = 1.37.

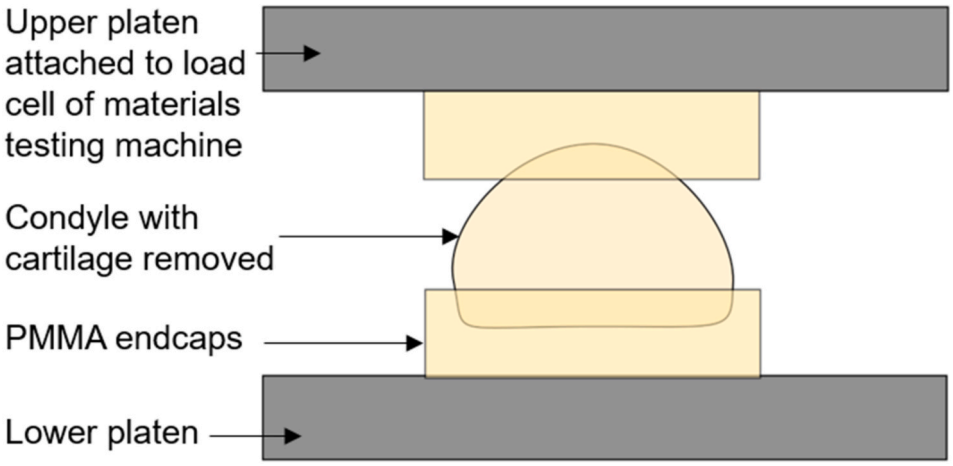

Fig. 2. Experimental setup for the testing of porcine condyles.

at a rate of 1 mm/min was applied to match the loading regime of the push-in tests. The load and displacement were recorded and the stiffness was measured by taking the average gradient between 200 and 500 N; this range was chosen as it gave comparable stresses to those in the FE models of the femoral condyles and the initial specimen specific FE push-in tests. A μCT scan of each specimen potted in its endcaps was taken prior to experimental loading with a HR-pQCT (XtremeCT, Scanco Medical AG, Switzerland; 82 μm isotropic voxel size: 900 lA, 60 kVp energy and 300 ms exposure).

2.1.2. Finite element methodology

FE models of the eight condyles were developed from the μCT scans. Models were segmented and meshed using Simpleware ScanIP (2019.09, Synopsis, USA). The μCT background was first binarised, using a fixed threshold across all specimens, and was then down-sampled to 0.164 mm^3, such that the resulting voxel greyscale was proportional to the bone volume fraction (Day et al., 2020). Bone materials were modelled as an isotropic linear elastic material, where the Young's modulus of each element was correlated with the greyscale value of the corresponding down-sampled voxel using a linear conversion factor (as in (Day et al., 2020) for similarly loaded and imaged vertebral specimens). The thresholded, binarised background was also used to calculate the bone volume fraction (BV/TV) for experimental specimen characterisation. FE models were solved using Abaqus (2017, Dassault Systèmes, France) by importing meshed geometries (linear tetrahedral elements, target edge length = 0.7 mm, approximately 108,000 elements) from Simpleware ScanIP. Elementwise material properties were applied using the Simpleware ScanIP greyscale based material property setup. All of the FE models developed for this study were quasi-static analyses, with geometric non-linearity. A relatively high mesh density was selected to allow for subsequent accurate modelling of the cylindrical holes and bone grafts. To check convergence, tests were carried out using homogeneous and inhomogeneous material properties. When the number of elements was doubled from that used, the change in stiffness was below 0.2% for the homogenous models and 1.5–3.3% for the models with inhomogeneous material properties. Linear element models were also compared to using quadratic elements, demonstrating their equivalence in this specific case (see data associated with the paper (Day et al., 2021)). Material properties for the PMMA endcaps used a Young's modulus of 2.45 GPa and a Poisson's ratio of 0.3 (McCormack et al., 1994). An encastre boundary condition was used on the inferior endcap, with a kinematic coupling applied to the superior endcap. The superior kinematic coupling received a 1 mm uniaxial displacement.

The relationship between the greyscale value and Young's modulus was optimised to provide the best fit, in a least square sense, between the FE-predicted stiffness values and the corresponding experimentally derived stiffness values. This was carried out using the opti4abq optimization toolbox (Mengoni, 2017).

2.2. Derivation of the coefficient of friction

Interactions between the graft and host were based on an iterative tuning of a simplified FE model based on published data (Bowland et al., 2020). The simplified model used homogenous material properties for

the bone, and models representing both bottomed (when the length of the graft was equal to the recipient site) and bottomless cases from the Bowland et al. study (Bowland et al., 2020) were generated. These models were not specimen specific, but were based on a μCT of a porcine femur, material properties are described in Table 1. In the Bowland et al. push-in force study, the force at 2 mm of graft displacement into the host was measured. This data was compared to the force measured in the FE models while iteratively changing the values of the coefficient of friction between the bone on bone, cartilage on bone, and cartilage on cartilage contacts.

The results of changing the coefficient of friction for the three contacts were tabulated and the optimum values were selected such that the mean error across the two cases, bottomed and bottomless was minimised.

2.3. Push-in model validation

2.3.1. Experimental model and imaging

Experimental testing was carried out on five porcine skeletally immature 4- to 6- month old femurs, utilising two of these femurs as donors from which to acquire osteochondral grafts. The samples were stored and kept hydrated with PBS as with the above condyles and all testing was completed within three days.

A surgical toolkit (Acufex Mosaicplasty, Smith & Nephew, UK) was used for the procedures. Two holes were drilled within each of the six porcine femoral condyles using a 6.35 mm diameter drill bit. Holes were drilled perpendicularly to the surface to a depth of 10 mm, using a hand-held drill with the femur held in a vice. Osteochondral grafts were harvested from the two donor knees using a 6.5 mm diameter chisel and a mallet, and then trimmed to 10 mm in length. Grafts were taken from a variety of locations, including both the condyles and the trochlear groove to provide grafts with a range of material properties and densities.

Computed tomography scans were taken for all five femurs before and after graft harvest for the donor knees and pre-hole and post-push in tests for the host knees. Scans were taken with the same HR-pQCT scanner and setting used above. The combination of scans enabled an exact determination of the locations and therefore properties of the grafts and host holes, which, in turn enabled specimen specific modelling of both the three host knees and the 12 grafts. The pre-harvest and post-test scans were also used to determine the host and graft bone volume fraction (BV/TV).

An experimental rig (Bowland et al., 2020) was used that allowed the positioning of the porcine femurs within a materials testing machine (Instron 3365 with a 5 kN load cell, Instron, UK) such that the grafts could be displaced axially within the holes in the femoral condyle (Fig. 3) (Bowland et al., 2020). The angle of the femur was adjusted so that the indentor attached to the head of the materials testing machine could be lowered into the drilled hole in the femur. This ensured that the push-in tests were conducted entirely axially. The head of the testing machine was then raised and the graft was inserted in the hole. A tamp was used to make the graft flush with the surrounding cartilage of the host femur. The 6 mm diameter indentor attached to the head of the materials testing machine was then lowered until it was in contact with the cartilage surface of the graft. A displacement of 2 mm was applied and the required force was measured.

2.3.2. Computational methodology

2.3.2.1. Description of the host femurs. Image registration, segmentation and FE meshing was carried out in Simpleware ScanIP (2019.09, Synopsis, USA). DICOM μCT scans were imported into Simpleware ScanIP where the two scans, before testing and after testing, were registered using an automatic workflow within the software and initial manual landmarking. The same thresholding, binarisation and down-sampling process described in Section 2.1.2, was used here. The reduced resolution from downsampling aided the segmentation of the cartilage and bone regions, which was achieved through a standardised thresholding

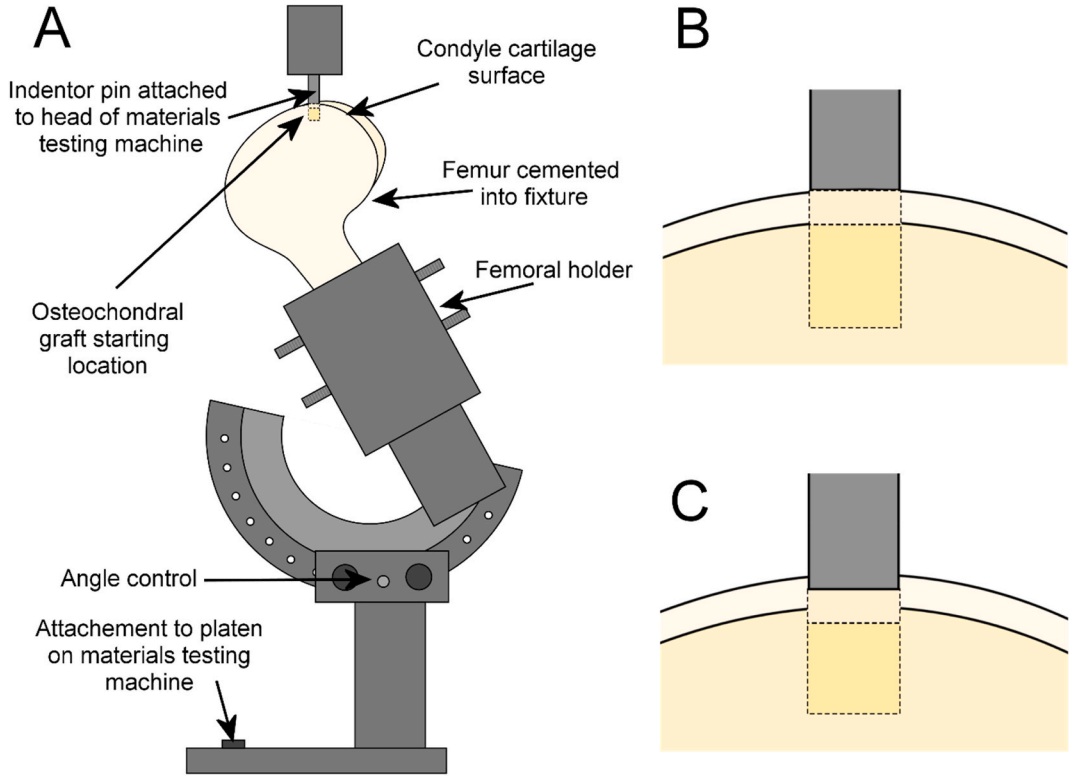

Fig. 3. A, the experimental set-up for push in tests using a porcine femur. B, the initial indentor and graft position flush with the surrounding host cartilage. C, the indentor and graft positioning following the application of a 2 mm displacement.

and morphological filtering process for all specimens. Mesh settings were identical to those used for the condyle material property derivation models, given the dependence of element size on the material properties. Material properties (Table 1) matched those used in Section 2.1, with the derived greyscale value to Young's modulus mapping.

2.3.2.2. Description of the osteochondral grafts and host holes. The grafts were defined using the surfaces tools in Simpleware ScanIP to match the experimental graft diameter, 6.5 mm, and graft length, 10 mm. The surfaces, when compared to segmented masks allowed for translation and rotation to the correct location and orientation based on the post-graft harvest scan. The voxel rendering options were used to aid the alignment, using the upper cartilage surface as the position of the top surface part. Material properties were assigned in a similar manner to the host models, by using the binarised pre-harvest image data, as shown in Fig. 4. The cylinders describing each graft were meshed using tetrahedral elements, with a target edge length of 1 mm. A 1 mm edge length produced a mesh with approximately 8032 elements, doubling the mesh density gave a difference in push-in force of 0.2% and using quadratic tetrahedral elements gave a difference of 0.6% while taking approximately 10 times as long to solve.

The holes (Fig. 5) within the host femoral condyles were created in a similar manner. Simpleware ScanIP surfaces were used to describe the holes (6.35 mm diameter), using the post-test scan to set the correct alignment and position and the pre-test scan to assign the correct material properties of the surrounding region. Contact surfaces were defined between the surface mesh, and the host bone and cartilage so that the mesh describing the hole had a high quality surface.

2.3.2.3. Finite element model setup. Using the pre-processing software in Abaqus, grafts were aligned with the holes based on the surface normal to the elements at the bottom of the host hole. To avoid the limitations of the built-in interference fit methodology, the graft was initially positioned outside of the host and displaced inwards until the cartilage surfaces were flush, at which point the displacement boundary condition was relaxed. A further 2 mm was then applied to the top graft surface, to replicate the experiment, and the reaction force was measured. The two step displacement conditions, separated by relaxing the boundary conditions, ensured that the cartilage layers were flush prior to the push-in displacement and therefore matched the experiment. The relaxation was required due to the graft oversizing. Fig. 6 shows the initial starting position of the graft, the end of the relaxation step and the final result. The remaining boundary condition was an encastre boundary applied to the superior surface of the host knee. The contacts between the different element sets used surface to surface hard contacts, with tangential friction and using values derived in Section 2.2.

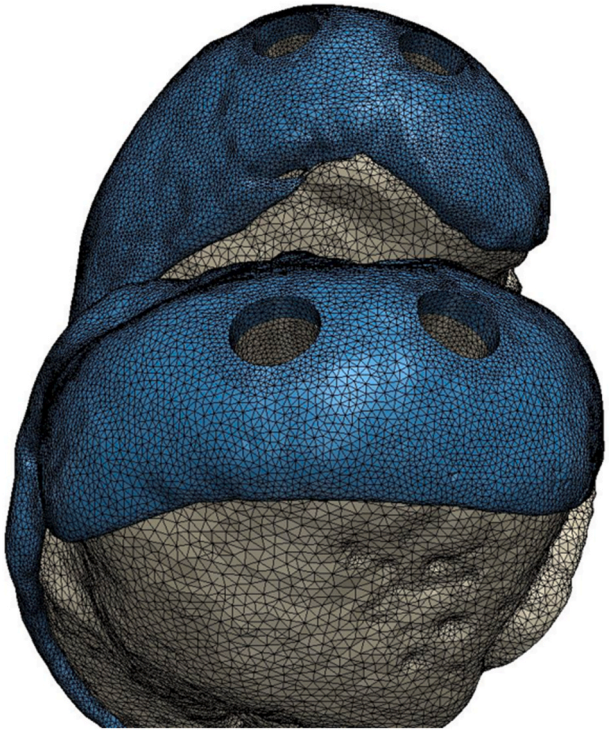

Fig. 5. FE model of Knee 1, showing bone and cartilage layers. Holes 4 and 2, respectively top left and top right, and holes 3 and 1, bottom left and bottom right.

A hyperelastic, neo-Hookean material property was used for the host and graft cartilage (Cooper et al., 2020), bulk modulus K = 16.67 MPa and shear modulus G = 1.37 MPa.

2.3.3. Sensitivity to oversizing and material properties

The sensitivity of the models to changing graft oversize was investigated by changing the graft diameter by ± 0.05 mm and ±0.1 mm. This change to the graft diameter also allowed testing of the model's ability to represent a wide range of possible outcomes. These tests were carried out on a single model (Knee 3, hole 4).

The dependence on the material properties of the grafts was investigated by, a) changing the Young's modulus of the graft elements to be homogeneous and uniform across the 12 tests and b) using specimen

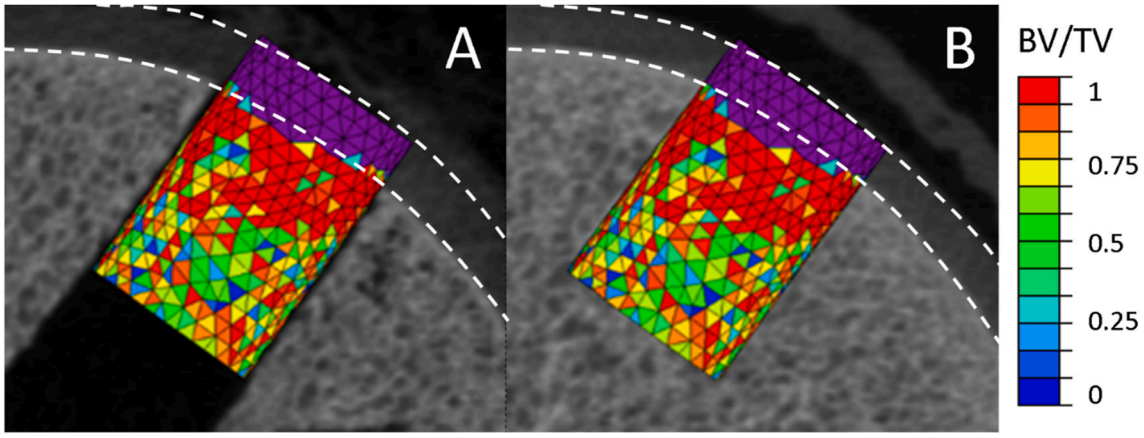

Fig. 4. The setup of the osteochondral graft meshes. A, the positioning of the graft according to the post-harvest μCT scan and B, the application of the material properties according to the pre-harvest scan. The scale indicates the effective BV/TV value for each element, with the top purple section representing the cartilage. The dashed white lines indicate the position of the host cartilage on the μCT scan.

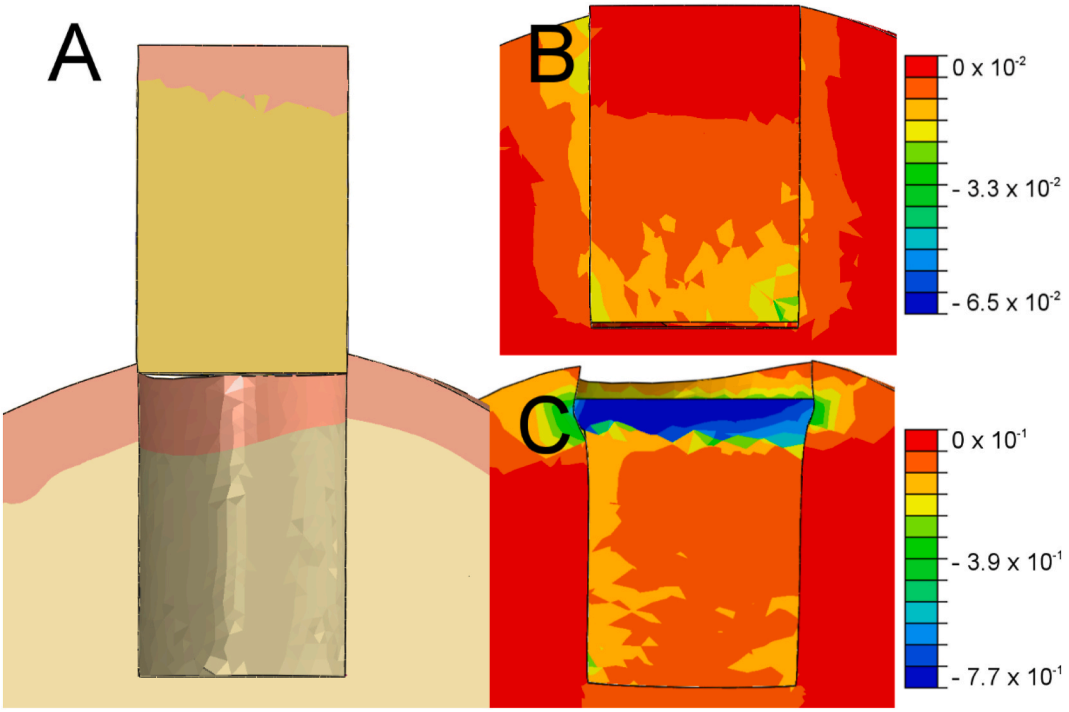

Fig. 6. Depiction of the push-in test. A, the graft in its initial step. B, the principal compressive strain (i.e. the magnitude of compressive strain taken in the direction where compressive strain is highest) following displacement and relaxation of the boundary conditions, showing the residual strain following the boundary condition relaxation. C, the principal compressive strain in the graft and host after the full 2 mm of displacement. Blue indicates high principal compressive strain and red indicates low principal compressive strain.

specific homogenous Young's modulus for the grafts. The former value was selected by using the average of the mean BV/TV value for each of the grafts (0.72) and multiplying it by the material mapping conversion factor, while the latter multiplied the mean BV/TV value of each graft by the conversion factor. These tests were carried out on all of the samples. These models used the same meshes as the other push-in tests with only the graft bone element material properties changed.

3. Results

The dataset associated with this study (3D images, experimental results, and computational models and scripts) is openly available from the University of Leeds data repository (Day et al., 2021).

3.1. Greyscale based material property calibration

A conversion factor between the brightness of each downsampled voxel (which was proportional to the local BV/TV) and the Young's modulus (E) of each element was achieved for the porcine condyles with an RMS error value of 9.2%. The experimental stiffness range was 1580 N/mm (790 N/mm to 2370 N/mm) and the range of errors when compared to the calibrated models was 0.6%–14%. The derived conversion factor was $E = 92.8 \times BV/TV$ (MPa). This was applied to each element of the host and graft meshes of the push-in test FE models.

3.2. Coefficient of friction calibration

The derived optimised coefficient of friction values were: 0.21 for bone on bone, 0.1 for cartilage on cartilage and 0.14 for bone on cartilage. The tabulated data for all coefficient of friction values investigated can be found in the associated dataset (Day et al., 2021). These values gave push-in force results of 234 N and 25 N, compared to experimental means of 190 N and 67 N (Bowland et al., 2020), for bottomed and bottomless respectively.

3.3. Experimental push-in results

Experimental push in results showed a relationship between the required push-in force at 2 mm and the bone volume fraction (BV/TV) of the grafts ($r^2 = 0.42$) (Fig. 7), the BV/TV of the host material ($r^2 = 0.19$) and the sum of the graft and host BV/TV ($r^2 = 0.48$). The experimental push-in force values ranged from 156 N to 416 N, with a mean of 300 N, Fig. 8. There was no significant difference found between the BV/TV or the push-in force for the grafts taken from the trochlear grove and the grafts taken from the condyles (Student's *t*-Test, $p = 0.071$).

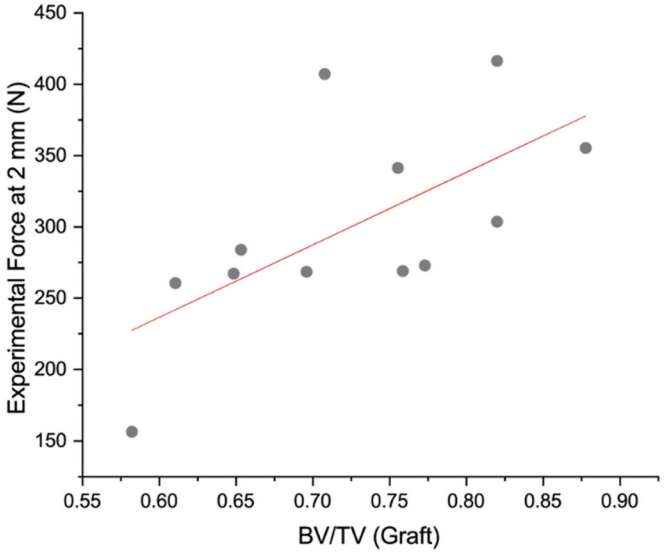

Fig. 7. The relationship between the force required to displace the grafts at 2 mm and the bone volume fraction of the graft bone ($r^2 = 0.42$).

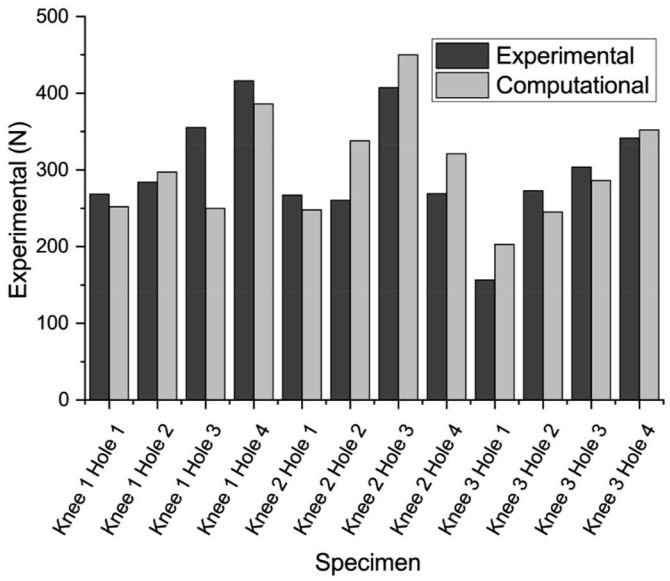

Fig. 8. The experimental and inhomogeneous specimen-specific computational results of the push-in force at 2 mm of displacement for the 12 grafts with a concordance correlation coefficient of 0.75.

3.4. Finite element validation

The agreement between the experimental push-in force and the specimen specific computational models was high (CCC = 0.75). Both high and low push-in forces were well represented, Fig. 8.

3.5. Sensitivity tests

The response of changing the graft diameter on the push-in force was linear with the force increasing with greater graft diameter ($r^2 = 0.998$). A reduction/increase in force of 24 N and 12 N was seen for changes of 0.1 mm and 0.05 mm respectively.

The effect of using specimen specific homogenous material properties and uniform homogenous material properties resulted in worse agreement with CCC values of 0.43 and 0.19 respectively, Table 2.

4. Discussion

A method of modelling the graft-host interaction has been developed and validated independently from the calibration of material and interaction properties. These models were found to be robust enough to vary the amount of graft oversizing without running into FE model convergence problems and could accurately represent a range of bone densities and distributions. The comparison of models with different approaches to describing the materials showed that a detailed description of the material mapping is required to accurately predict the push-in forces.

The representation of the graft oversizing within the models was challenging. Modelling methodologies that used the built-in interference fit within Abaqus were found to be unreliable when using specimen specific, image-space based meshes and presented limitations on the amount of oversizing for geometric part based meshes. Examples of models exhibiting the interference fit limitations are contained in the associated dataset (Day et al., 2021). Other options were investigated, such as an outward radial pressure applied to a non-oversized graft, however the radial pressure proved difficult to tune in order to replicate various oversizes. The settled upon method presented in this study allowed for matching of the experimental oversizing and the models converged reliably so long as the graft alignment for the initial displacement step was ensured. The only disadvantage was the computational cost of running two extra steps, the first to displace the graft into the host and the second to relax the displacement boundary condition applied to the graft's cartilage surface. While these extra steps accounted for between half and three quarters of the total iterations, the average simulation time was only 45 min compared to the 6 h of the comparable explicit analysis of Ovesy et al. (2020).

Table 2
The effect of material property description method on the concordance correlation coefficient.

Method	Concordance Correlation Coefficient
Specimen Specific Greyscale	0.75
Specimen Specific Homogenous (0.72 × BV/TV MPa)	0.43
Uniform Homogenous (E = 67 MPa)	0.28

Despite the requirement for the models to have high quality contact surfaces in order to reliably solve with a wide range of material properties and oversizing, the experimental roughness of the grafts was still captured in the models. This was done through three features of the grafts. The first of these was the graft oversizing, contributing to the normal force of the graft surface acting on the host bone. The second was the varying element Young's modulus of the grafts and host bone at their interface. The variation here leads to a varying normal force for each element. The final component is the coefficient of friction value for the different materials. While this was tuned on simpler models, the ability to describe the bottomed and bottomless (interference fit in isolation) cases proved to be adequate for the more detailed specimen specific models. It should be noted that the derived coefficient of friction is only valid for models employing the same approach, and with similar element sizes. The coefficient of friction between the cartilage surfaces of the graft and host (0.1) was higher than that reported in other studies where frictionless or near frictionless surfaces are often described for the joint surfaces (D'Lima D et al., 2009; Kazemi et al., 2012; Park et al., 2019; Guo et al., 2017). However, in osteochondral graft models where cut, transverse edges are in contact, values of 0.1 and higher have been used (Heuijerjans et al., 2018; Lane et al., 2009). In any case, sensitivity to this particular interaction was small, for example with Knee 1 Hole 1, differences of 0.16% were measured when using a value of 0.01 compared to the 0.1 value used in the study (251.6 N vs 252.0 N respectively) and a difference of 0.16% when using a value of 0.2 compared to the 0.1 value (252.4 N vs 252.0 N respectively). Using the larger value for the coefficient improved the stability of the models and resulted in more consistent model convergence in addition to reduced computation time.

Experimentally, the relationship between the density or BV/TV of the grafts and host, and the required push-in force was weak, especially between the host density and the push-in force. The somewhat stronger relationship between graft and the push-in force can be postulated to be due to the compression of the graft within the host and hence the force measured was more dependent on the properties of the graft. The importance of representing the material properties of the grafts in detail, rather than homogeneous properties, was shown when comparing approaches to describing the bone with the FE models. Homogenous bone, both specimen specific or uniform, performed considerably worse in representing the push-in force, aligning with the weak correlations within the experimental data. This suggests that homogenous properties are insufficient to accurately predict the push-in force. These results show the value and necessity of having models with accurate material property mapping compared to homogenous based models that are often used in the literature (D'Lima D et al., 2009; Wu et al., 2002; Heuijerjans et al., 2018; Papaioannou et al., 2010). While the results of Heuijerjans et al. (2018) suggests that graft angle rather than the material properties have a more important role in osteochondral grafting, their results may change or be improved upon with specimen specific material properties and an accurate representation of graft oversizing. These results also

agree with those of Venäläinen et al. (2016), who found that CT derived material properties changed the stress distribution within articular cartilage and were necessary to fully describe the mechanical effects of the cartilage within the tibiofemoral joint. The material calibration constant itself produced material properties with comparable Young's modulus ranges to those found in the literature for similar human trabecular bone (Heuijerjans et al., 2018; Venäläinen et al., 2016; Peng et al., 2006) and porcine trabecular bone (Koria et al., 2020).

The response of the computational push-in force to changing graft oversizing was linear, giving a uniform increase to the force required for each step in graft size. This follows from an analytical standpoint, where the force from friction is linearly proportional to the normal force and the normal force is linearly proportional to the change in graft radius (and therefore oversize). The slight variations away from a linear relationship are likely due to changes in the material properties of the graft when its diameter was changed.

These models of push-in testing and the approaches used to create them are well validated for the experimental conditions. The models were developed assessing their capacity to replicate experimental forces (compression force or push-in force depending on the type of model). While the forces were chosen to simulate stress values in the same range for both type of models, this does not inform on the validity of the stress or strain values obtained which are outside their context of use. As such, the methodology developed here can be used to examine the short term stability of osteochondral grafts and assess the effect of a range of surgical variables.

The remaining challenges surround the adaption of the methodology to work with cadaveric human tissue and in the tibiofemoral joint. The push-in forces of porcine specimens in this and previous studies (Bowland et al., 2020), and those in the literature using human tissue (Kock et al., 2008, 2011) are similar, suggesting that the methodologies will remain appropriate. The use of similar hyperelastic material properties for the articulating cartilage surfaces to those used in models of Cooper et al. (2020) also promises an easy transition into models of full tibiofemoral joints, given that these models will require different contact conditions and larger applied loads than those in the current study. Although the cartilage properties have little effect on the stability compared to the stiffer bone properties, the cartilage thickness is likely to affect contact mechanics, so the explicit representation of this layer in these models is also important. While numerous studies have investigated the effect of inhomogenous material properties (Venäläinen et al., 2016), the role of ligaments (Lane et al., 2009; Papaioannou et al., 2010) and other factors affecting the FE modelling of tibiofemoral joints (Cooper et al., 2019, 2020; Guo et al., 2017; Venäläinen et al., 2016), little research has incorporated osteochondral grafting into these environments. Models of grafts within a specimen specific tibiofemoral joint would be able to provide data on the effect of graft angle (akin to (Heuijerjans et al., 2018)), materials, proudness, and hole preparation on metrics of graft stability, such as graft circumferential contact pressure, push-in force, and articular cartilage contact pressure.

5. Conclusion

Changes to the material properties of the grafts, beyond metrics of the bulk material, have been shown to have large effects on the push-in force required. This change to the push-in force and therefore initial stability of the grafts may influence the likelihood of procedure success, due to both risk of subsidence and damage to opposing articular cartilage. The novel and robust FE method developed will allow for a detailed study into patient, graft and procedural variation.

CRediT authorship contribution statement

Gavin A. Day: Writing – review & editing, Writing – original draft, Visualization, Validation, Software, Methodology, Investigation, Formal analysis, Data curation, Conceptualization. **Robert J. Cooper:** Writing – review & editing, Visualization, Investigation, Data curation, Conceptualization. **Alison C. Jones:** Writing – review & editing, Visualization, Supervision, Project administration, Conceptualization. **Marlène Mengoni:** Writing – review & editing, Visualization, Supervision, Project administration, Conceptualization. **Ruth K. Wilcox:** Writing – review & editing, Visualization, Supervision, Project administration, Funding acquisition, Conceptualization.

Declaration of competing interest

The authors declare that they have no known competing financial interests or personal relationships that could have appeared to influence the work reported in this paper.

Data availability

Data is available through the University of Leeds Library website, a DOI will be minted upon acceptance, references are already in place within the document.

Acknowledgements

This work was funded by the EPSRC (grant number EP/P001076/1).

References

Becher, C., Huber, R., Thermann, H., Paessler, H.H., Skrbensky, G., 2008. Effects of a contoured articular prosthetic device on tibiofemoral peak contact pressure: a biomechanical study. Knee Surg. Sports Traumatol. Arthrosc. 16, 56–63. https://doi.org/10.1007/s00167-007-0416-7.

Bortoluzzi, A., Furini, F., Scirè, C.A., 2018. Osteoarthritis and its management - epidemiology, nutritional aspects and environmental factors. Autoimmun. Rev. 17, 1097–1104. https://doi.org/10.1016/j.autrev.2018.06.002.

Bowland, P., Ingham, E., Fisher, J., Jennings, L.M., 2018a. Simple geometry tribological study of osteochondral graft implantation in the knee. Proc. IME H J. Eng. Med. 232, 249–256. https://doi.org/10.1177/0954411917751560.

Bowland, P., Ingham, E., Fisher, J., Jennings, L.M., 2018b. Development of a preclinical natural porcine knee simulation model for the tribological assessment of osteochondral grafts in vitro. J. Biomech. 77, 91–98. https://doi.org/10.1016/j.jbiomech.2018.06.014.

Bowland, P., Cowie, R.M., Ingham, E., Fisher, J., Jennings, L.M., 2020. Biomechanical assessment of the stability of osteochondral grafts implanted in porcine and bovine femoral condyles. Proc. IME H J. Eng. Med. 234, 163–170. https://doi.org/10.1177/0954411919891673.

Cooper, R.J., Wilcox, R.K., Jones, A.C., 2019. Finite element models of the tibiofemoral joint: a review of validation approaches and modelling challenges. Med. Eng. Phys. 74, 1–12. https://doi.org/10.1016/j.medengphy.2019.08.002.

Cooper, R.J., Liu, A., Day, G.A., Wijayathunga, V.N., Jennings, L.M., Wilcox, R.K., Jones, A.C., 2020. Development of robust finite element models of porcine tibiofemoral joints loaded under varied flexion angles and tibial freedoms. J. Mech. Behav. Biomed. Mater. 109 https://doi.org/10.1016/j.jmbbm.2020.103797.

Crawford, D.C., Miller, L.E., Block, J.E., 2013. Conservative management of symptomatic knee osteoarthritis: a flawed strategy? Orthop. Rev. 5, 2. https://doi.org/10.4081/or.2013.e2.

Custers, R.J.H., Dhert, W.J.A., van Rijen, M.H.P., Verbout, A.J., Creemers, L.B., Saris, D. B.F., 2007. Articular damage caused by metal plugs in a rabbit model for treatment of localized cartilage defects. Osteoarthritis Cartilage 15, 937–945. https://doi.org/10.1016/j.joca.2007.02.007.

Day, G.A., Jones, A.C., Wilcox, R.K., 2020. Optimizing computational methods of modeling vertebroplasty in experimentally augmented human lumbar vertebrae. Jor Spine 3. https://doi.org/10.1002/jsp2.1077.

Day, G.A., Cooper, R.J., Jones, A.C., Mengoni, M., Wilcox, R.K., 2022. Stability of Osteochondral Grafts within Porcine Femoral Condyles - experimental, imaging and computational data for preclinical assessment. University of Leeds. https://doi.org/10.5518/1209.

D'Lima D, D., Chen P, C., Colwell Jr., W., 2009. Osteochondral grafting: effect of graft alignment, material properties, and articular geometry. Open Orthop. J. 3, 61–68. https://doi.org/10.2174/1874325000903010061. C.

Guo, H., Santner, T.J., Lerner, A.L., Maher, S.A., 2017. Reducing uncertainty when using knee-specific finite element models by assessing the effect of input parameters. J. Orthop. Res. 35, 2233–2242. https://doi.org/10.1002/jor.23513.

Heuijerjans, A., Wilson, W., Ito, K., van Donkelaar, C.C., 2018. Osteochondral resurfacing implantation angle is more important than implant material stiffness. J. Orthop. Res. 36, 2911–2922. https://doi.org/10.1002/jor.24101.

Hunziker, E.B., 2002. Articular cartilage repair: basic science and clinical progress. A review of the current status and prospects. Osteoarthritis Cartilage 10, 432–463. https://doi.org/10.1053/joca.2002.0801.

Kazemi, M., Li, L.P., Buschmann, M.D., Savard, P., 2012. Partial meniscectomy changes fluid pressurization in articular cartilage in human knees. J. Biomech. Eng. 134 https://doi.org/10.1115/1.4005764.

Kirker-Head, C.A., Van Sickle, D.C., Ek, S.W., McCool, J.C., 2006. Safety of, and biological and functional response to, a novel metallic implant for the management of focal full-thickness cartilage defects: preliminary assessment in an animal model out to 1 year. J. Orthop. Res. 24, 1095–1108. https://doi.org/10.1002/jor.20120.

Kock, N.B., Smolders, J.M.H., Van Susante, J.L.C., Buma, P., Van Kampen, A., Verdonschot, N., 2008. A cadaveric analysis of contact stress restoration after osteochondral transplantation of a cylindrical cartilage defect. Knee Surg. Sports Traumatol. Arthrosc. 16, 461–468. https://doi.org/10.1007/s00167-008-0494-1.

Kock, N.B., Hannink, G., van Kampen, A., Verdonschot, N., van Susante, J.L.C., Buma, P., 2011. Evaluation of subsidence, chondrocyte survival and graft incorporation following autologous osteochondral transplantation. Knee Surg. Sports Traumatol. Arthrosc. 19, 1962–1970. https://doi.org/10.1007/s00167-011-1650-6.

Koh, J.L., Wirsing, K., Lautenschlager, E., Zhang, L.O., 2004. The effect of graft height mismatch on contact pressure following osteochondral grafting: a biomechanical study. Am. J. Sports Med. 32, 317–320. https://doi.org/10.1177/0363546503261730.

Koh, J.L., Kowalski, A., Lautenschlager, E., 2006. The effect of angled osteochondral grafting on contact pressure a biomechanical study. Am. J. Sports Med. 34, 116–119. https://doi.org/10.1177/0363546505281236.

Koria, L., Mengoni, M., Brockett, C., 2020. Estimating tissue-level properties of porcine talar subchondral bone. J. Mech. Behav. Biomed. Mater. 110, 103931 https://doi.org/10.1016/j.jmbbm.2020.103931.

Lane, J., Healey, R., Amiel, D., 2009. Changes in condylar coefficient of friction after osteochondral graft transplantation and modulation with hyaluronan. Arthrosc. J. Arthrosc. Relat. Surg. 25, 1401–1407. https://doi.org/10.1016/j.arthro.2009.04.074.

Manda, K., Ryd, L., Eriksson, A., 2011. Finite element simulations of a focal knee resurfacing implant applied to localized cartilage defects in a sheep model. J. Biomech. 44, 794–801. https://doi.org/10.1016/j.jbiomech.2010.12.026.

Martinez-Carranza, N., Berg, H.E., Hultenby, K., Nurmi-Sandh, H., Ryd, L., Lagerstedt, A. S., 2013. Focal knee resurfacing and effects of surgical precision on opposing cartilage. A pilot study on 12 sheep. Osteoarthritis Cartilage 21, 739–745. https://doi.org/10.1016/j.joca.2013.02.004.

McCormack, T., Karaikovic, E., Gaines, R.W., 1994. The load sharing classification of spine fractures. Spine 19, 1741–1744. https://doi.org/10.1097/00007632-199408000-00014.

Mengoni, M., 2017. opti4Abq (V 2.0), a Generic python Code to Run Abaqus in an Optimisation Loop. https://doi.org/10.5281/zenodo.580475. See.

Ovesy, M., Aeschlimann, M., Zysset, P.K., 2020. Explicit finite element analysis can predict the mechanical response of conical implant press-fit in homogenized trabecular bone. J. Biomech., 109844 https://doi.org/10.1016/j.jbiomech.2020.109844.

Papaioannou, G., Demetropoulos, C.K., King, Y.H., 2010. Predicting the effects of knee focal articular surface injury with a patient-specific finite element model. Knee 17, 61–68. https://doi.org/10.1016/j.knee.2009.05.001.

Park, S., Lee, S., Yoon, J., Chae, S.W., 2019. Finite element analysis of knee and ankle joint during gait based on motion analysis. Med. Eng. Phys. 63, 33–41. https://doi.org/10.1016/j.medengphy.2018.11.003.

Pearce, S.G., Hurtig, M.B., Clarnette, R., Kalra, M., Cowan, B., Miniaci, A., 2001. An investigation of 2 techniques for optimizing joint surface congruency using multiple cylindrical osteochondral autografts. Arthroscopy. https://doi.org/10.1053/jars.2001.19966.

Peng, L., Bai, J., Zeng, X., Zhou, Y., 2006. Comparison of isotropic and orthotropic material property assignments on femoral finite element models under two loading conditions. Med. Eng. Phys. 28, 227–233. https://doi.org/10.1016/j.medengphy.2005.06.003.

Seo, S., Kim, C., research DJ-K surgery & related, 2011. Management of Focal Chondral Lesion in the Knee Joint. ncbi.nlm.nih.Gov undefined. (in press).

Venäläinen, M.S., Mononen, M.E., Väänänen, S.P., Jurvelin, J.S., Töyräs, J., Virén, T., Korhonen, R.K., 2016. Effect of bone inhomogeneity on tibiofemoral contact mechanics during physiological loading. J. Biomech. 49, 1111–1120. https://doi.org/10.1016/j.jbiomech.2016.02.033.

Wu, J.Z., Herzog, W., Hasler, E.M., 2002. Inadequate placement of osteochondral plugs may induce abnormal stress-strain distributions in articular cartilage - finite element simulations. Med. Eng. Phys. 24, 85–97. https://doi.org/10.1016/S1350-4533(01)00122-9.

Zhao, S., Arnold, M., Ma, S., Abel, R.L., Cobb, J.P., Hansen, U., Boughton, O., 2018. Standardizing compression testing for measuring the stiffness of human bone. Bone Joint. Res. 7, 524–538. https://doi.org/10.1302/2046-3758.78.BJR-2018-0025.R1.